Selective Adsorption of Sulfur Dioxide in a Robust Metal-Organic Framework Material

Document Version
Final published version

Selective Adsorption of Sulfur Dioxide in a Robust Metal–Organic Framework Material

Mathew Savage, Yongqiang Cheng, Timothy L. Easun, Jennifer E. Eyley, Stephen P. Argent, Mark R. Warren, William Lewis, Claire Murray, Chiu C. Tang, Mark D. Frogley, Gianfelice Cinque, Junliang Sun, Svemir Rudić, Richard T. Murden, Michael J. Benham, Andrew N. Fitch, Alexander J. Blake, Anibal J. Ramirez-Cuesta, Sihai Yang,* and Martin Schröder*

There is ever-increasing concern over global air quality, with high concentrations of smog posing significant health risks worldwide, particularly in major cities with heavy industry and high population densities. The World Health Organization (WHO) suggests that

Dr. M. Savage, J. E. Eyley, Dr. S. Yang, Prof. M. Schröder
School of Chemistry
University of Manchester
Manchester M13 9PL, UK
E-mail: Sihai.Yang@manchester.ac.uk;
M.Schroder@manchester.ac.uk
Dr. Y. Cheng, Dr. A. J. Ramirez-Cuesta
The Chemical and Engineering Materials Division (CEMD)
Neutron Sciences Directorate
Oak Ridge National Laboratory
Oak Ridge, TN 37831, USA
Dr. T. L. Easun
School of Chemistry
Cardiff University
Cardiff CF10 3XQ, UK
Dr. S. P. Argent, Dr. W. Lewis, Prof. A. J. Blake
School of Chemistry
University of Nottingham
University Park
Nottingham NG7 2RD, UK
Dr. M. R. Warren, Dr. C. Murray, Prof. C. C. Tang,
Dr. M. D. Frogley, Dr. G. Cinque
Diamond Light Source
Harwell Science Campus
Oxfordshire OX11 0DE, UK
Prof. J. Sun
College of Chemistry and Molecular Engineering
Peking University
Beijing 100871, China
Dr. S. Rudić
ISIS Neutron & Muon Source
STFC Rutherford Appleton Laboratory
Chilton, Oxfordshire OX11 0QX, UK
R. T. Murden, Dr. M. J. Benham
Hiden Isochema
422 Europa Boulevard, Warrington WA5 7TS, UK
Dr. A. N. Fitch
European Synchrotron Radiation Facility
Grenoble 38043, France

poor air quality is directly responsible for one eighth of total global deaths.[1] The problem posed by smog is particularly pronounced in Asia, where it is responsible for over 500 000 premature deaths every year.[2] Smog is comprised primarily of hydrocarbons, particulates, and oxides of nitrogen and sulfur, which are emitted as byproducts of combustion in both transportation and industrial applications. Emissions of sulfur dioxide (SO_2) from industrial applications are increased by the burning of coal and lower-grade oil, which have a high concentrations of sulfur.[3] Selective removal of SO_2 from the combustion flue gas is therefore of fundamental importance to the improvement of air quality.

Typical flue gas generated by the combustion of pulverized coal can contain 10–12% CO_2, 500–3000 ppm SO_2, and 10–40 ppm NO_2.[4] The majority of the SO_2 present in the flue gas (≈95%) can be removed by processes such as scrubbing with limestone slurry or the via the wet sulfuric acid process.[5] Although these industrial processes have high efficiency and are cost effective, they are not able to remove all traces of SO_2. Residual SO_2 in post-combustion flue gas can react with organic amines in the CO_2 scrubbing process, causing permanent loss of amine activity and decreasing the efficiency of this process. Emissions of SO_2 following all post combustion processing can be as high as 400 ppm, which when vented to the atmosphere is 50 000 times higher than the WHO recommendation of 8 ppb, and therefore poses a significant health risk.[6] Complete removal of traces of SO_2 is challenging since it requires capture systems possessing exceptionally high selectivity of SO_2 over N_2 and CO_2 and simultaneously considerable stability given the highly corrosive and reactive nature of SO_2.[7]

Reversible physisorption within porous materials provides a promising approach for selective gas removal. Constructed from organic ligands and metal ions, metal–organic framework (MOF) materials have been studied widely for gas adsorption over the past decade owing to their high internal surface area and porosity.[8] The highly modular nature of these framework solids allows the design of materials tuned with specific functional groups and/or open metal sites for specific binding to guest molecules within the pore. For this reason, MOFs have shown great promise in applications such as gas adsorption, storage, and separation, substrate binding, and drug delivery.[9] Within the field of gas adsorption, major research interest has been focused on using MOFs for high capacity storage of hydrogen and methane, and for the separation of CO_2 and small molecule hydrocarbons.[9a,10,11] However, in contrast, studies on adsorption of SO_2 in MOFs have been very rarely reported[12]

due to the limited stability of coordination compounds to highly reactive SO_2; this is particularly the case for MOFs with open metal sites and this has precluded the study of adsorption of this important pollutant. Herein, we report the selective SO_2 adsorption in an ultra-robust MOF material [MFM-300(In)] with high adsorption capacity of SO_2 (8.28 mmol g^{-1} at 298 K and 1 bar) and, more importantly, exceptionally high selectivity of SO_2/CO_2 (60), SO_2/CH_4 (425), and SO_2/N_2 (5000) under ambient conditions (i.e., 50:50 mixture at 1 bar and 298 K). The material can be readily regenerated post-adsorption without incurring any noticeable framework degradation. We also report the direct observation and quantification of adsorbed SO_2, CO_2, and N_2 molecules in the pore of this material in order to understand this unusually high selectivity. The nature of the host–guest binding interactions have been systematically studied by a combination of in situ single-crystal and powder X-ray diffraction, infrared microspectroscopy and inelastic neutron scattering (INS) experiments, coupled with computational modeling. These complementary techniques give consistent results confirming that adsorbed SO_2 forms specific multiple supramolecular interactions with the free hydroxyl groups and aromatic rings on the pore surface of this material, with significantly weakened interactions in the case of CO_2 and N_2 adsorption, thus rationalizing the observed selectivities at a molecular level.

The complex MFM-300(In) (MFM = Manchester Framework Material replacing the previous NOTT (Nottingham) designation) [In$_2$(OH)$_2$(L)] (H$_4$L = biphenyl-3,3′,5,5′-tetracarboxylic acid) was synthesized by solvothermal reaction of In(NO$_3$)$_3$ and H$_4$L in DMF (N,N-dimethylformamide) at 90 °C.[11] MFM-300(In)

is isostructural to MFM-300(Al)[12a] and MFM-300(Ga),[13] and comprises chains of corner sharing [InO$_4$(OH)$_2$] octahedra linked by mutually cis-μ$_2$-OH groups, and further bridged by tetracarboxylate L^{4-} ligands. This arrangement generates a highly porous material, defined by one-dimensional pore channels bounded by In-OH-In groups and ligand phenyl rings in a "wine rack" array. Desolvated MFM-300(In) displays a Brunauer–Emmett–Teller (BET) surface area of 1071 m^2 g^{-1}, a pore size of ≈7.5 Å, and a total pore volume of 0.419 cc g^{-1} as determined from N$_2$ isotherm at 77 K. Desolvated MFM-300(In) shows a very high concentration of functional groups in the pore; there are approximately two hydroxyl groups per 100 Å^2 internal surface area.

Adsorption of N$_2$, CO$_2$, and SO$_2$ as single component gases in MFM-300(In) exhibit reversible type-I isotherms over a wide temperature range between 298 and 348 K (**Figure 1**a,b and Figure S10–S14, Supporting Information) with significantly different adsorption capacities. At all temperatures, the adsorption of SO$_2$ is strongly favored within this material. At 298 K, MFM-300(In) shows a steep SO$_2$ adsorption profile between 0 and 50 mbar leading to an uptake of 5.90 mmol g^{-1} accounting for 71% of the maximum uptake of 8.28 mmol g^{-1} recorded at 1 bar. In contrast, the uptake of CO$_2$ and N$_2$ in MFM-300(In) are recorded as 3.61 and 0.25 mmol g^{-1}, respectively, at 298 K and 1 bar. Importantly, the low pressure region of the CO$_2$ isotherm shows a much lower adsorption uptake (0.18 mmol g^{-1} at 50 mbar) than that of SO$_2$ uptake (5.90 mmol g^{-1}), while the uptake of N$_2$ is negligible (<0.05 mmol g^{-1}) under the same conditions, confirming the high affinity of MFM-300(In) to SO$_2$.
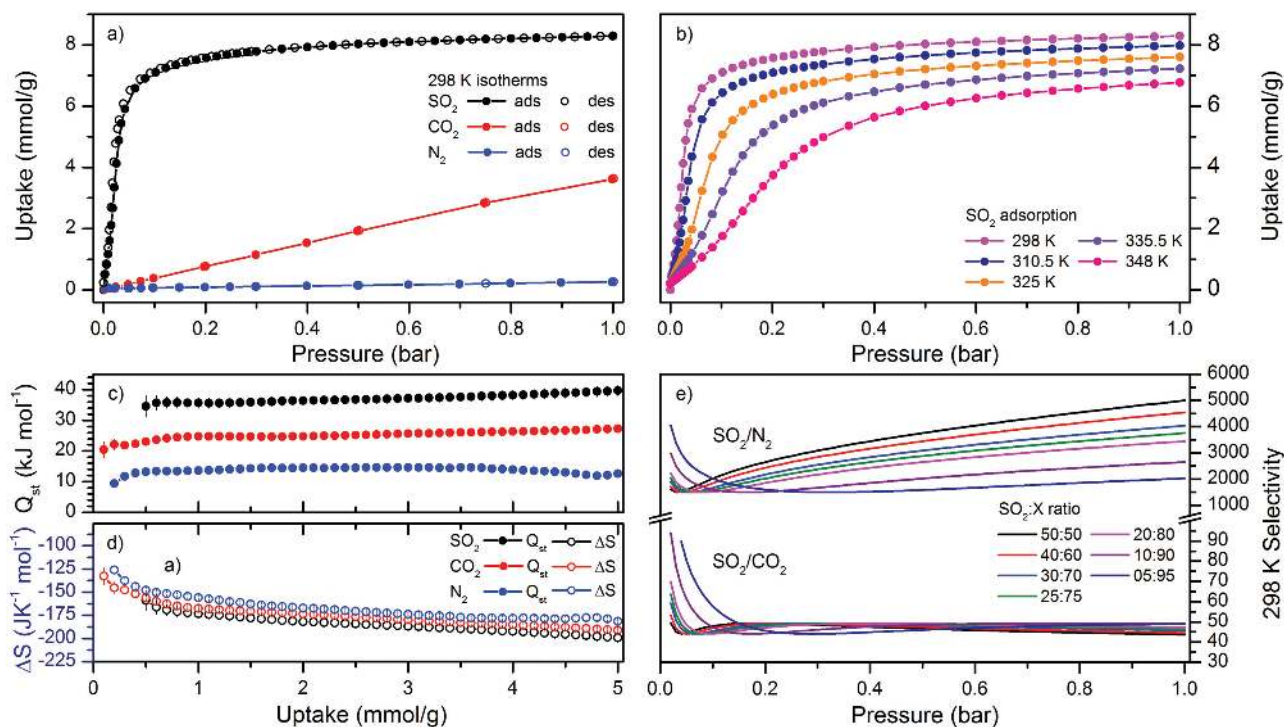

Figure 1. View of a) N$_2$, CO$_2$, and SO$_2$ adsorption isotherms of MFM-300(In) to a pressure of 1 bar at 298 K; b) SO$_2$ adsorption isotherms of MFM-300(In) between 298 and 348 K; c,d) isosteric heat and entropy of adsorption for N$_2$, CO$_2$, and SO$_2$ in MFM-300(In); e) IAST selectivity of SO$_2$/N$_2$ and SO$_2$/CO$_2$ mixtures in MFM-300(In) to a pressure of 1 bar at 298 K.

Under the same conditions, the uptake of CH_4 in MFM-300(In) is also low (Figure S17, Supporting Information). Adsorption of SO_2 in MFM-300(In) reduces steadily as the temperature increases from 298 to 348 K, consistent with the nature of physisorption. Nevertheless, at 348 K, a high SO_2 uptake of 6.78 mmol g^{-1} was recorded in MFM-300(In) at 1 bar. At 298 K and 1 bar, the SO_2 uptake of MFM-300(In) (8.28 mmol g^{-1}) is higher than that of MFM-300(Al) (7.1 mmol g^{-1}),[12a] but lower than that of MFM-202a (10.2 mmol g^{-1}),[12b] which has a much higher surface area of 2220 m^2 g^{-1}. However, adsorption of SO_2 in MFM-202a triggers an irreversible framework phase transition in addition to a shallower adsorption profile in the low pressure region in comparison to that of MFM-300(In). The SO_2 adsorption capacity of MFM-300(In) is significantly higher than that reported for other sorbent materials, including the very stable Prussian blue analogues ZnCo and CoCo (1.8 and 2.5 mmol g^{-1} at 1 bar and 298 K, respectively)[12d] and other MOF materials such as IRMOF-3, MOF-74, and MOF-5 (6.0, 3.0, and 1.0 mmol g^{-1}, respectively at 298 K and 1 bar).[12c] The isosteric heat (Q_{st}) and entropies (ΔS) of adsorption were determined by fitting of the Van't Hoff isochore to the adsorption isotherms of each gas at at least 5 temperatures (Figure 1c,d, Figure S15, Supporting Information). In order to accurately compare these values at all surface coverages, high pressure N_2 adsorption isotherms were recorded up to 180 bar at ambient temperatures, where a coverage of *ca.* 5 mmol g^{-1} was reached (Figure S11, Supporting Information). MFM-300(In) shows a low Q_{st} for N_2 of 9.4 kJ mol^{-1} at low surface coverage, rising to 14.6 kJ mol^{-1} at 4.0 mmol g^{-1}, significantly lower than that of CO_2 with a Q_{st} of 20.3 kJ mol^{-1} at low loading, rising to 27.2 kJ mol^{-1} at 5 mmol g^{-1}. In contrast, the Q_{st} for SO_2 is considerably higher, with a value of 34.5 kJ mol^{-1}, increasing to 39.6 kJ mol^{-1} at 5 mmol g^{-1}, representing the highest value observed in MOF materials.[12] A steady increase in the isosteric heats of adsorption was observed for all three gases suggesting the presence of strong adsorbate–adsorbate interaction in the pore as the surface coverage increases.

The marked differences in adsorption profiles, uptake capacities, and Q_{st} between SO_2, CO_2, CH_4, and N_2 indicates that MFM-300(In) has the potential to separate mixtures of these gases. To provide further insight into the potential separation capability of this material, ideal adsorbed solution theory (IAST) calculations[14] was carried out for SO_2/CO_2, SO_2/CH_4, and SO_2/N_2 gas mixtures in MFM-300(In) as a function of pressure and over a range of molar compositions (from 5:95 to 50:50), representative of a wide range of potential applications (Figure 1e and Figure S18, Supporting Information). It is important to note that IAST calculations based upon mixtures with ratios below 5:95 give artificially high selectivity values, which are subject to high uncertainties and are therefore not reported here. The selectivity data for SO_2/CO_2 and SO_2/CH_4 are between 46–60 and 275–425, respectively, and are relatively constant as a function of pressure and gas stream composition. Crucially, MFM-300(In) shows an extremely high SO_2/N_2 selectivity of 5000 at 1 bar, representing the highest value observed to date.[12] It is worth noting that IAST calculations often overestimate the selectivity if one adsorbate is strongly favored over another and can only give a theoretical insight into the separation capability of a given material. To overcome this problem,

we used isotherm data for N_2 up to 180 bar in order to obtain comparable spreading pressure data to that of SO_2 and therefore perform reliable IAST calculations. Indeed, we have tried to perform the IAST calculations of SO_2/N_2 selectivity based upon N_2 isotherm up to 1 and 20 bar, where the selectivities were overestimated by ≈10× and ≈3× (Figure S18, Supporting Information), respectively. The unprecedented selectivity of MFM-300(In) for SO_2 confirms its potential as an adsorbent for selective SO_2 removal, particularly in applications where low residual SO_2 is of prime importance.

Direct observation of adsorbed gas molecules within the MFM-300(In) host material is essential in order to gain a molecular understanding of the high selectivity of this material. In this study, the locations of adsorbed SO_2 and CO_2 molecules in MFM-300(In) have been determined unambiguously by in situ synchrotron powder or single-crystal X-ray diffraction experiments (**Figure 2**). Two independent SO_2 adsorption sites (SO_2^I and SO_2^{II}) were found in SO_2-loaded MFM-300(In) at 298 K (Figure 2a–c). Specifically, SO_2^I is located near to the bridging hydroxyl group, [O=S=O^I···O−H = 3.17(4) Å] with full site occupancy; SO_2^{II} is located perpendicular to SO_2^I [O=S=O^{II}···S=O^I = 4.52(2) Å] and parallel within the pore at a distance of 3.92(5) Å from the phenyl rings, also with full site occupancy. The O=S=O^I···O−H and O=S=O^{II}···S=O^I interaction distances within this material were observed to be within the same range as in the pure component crystal structure of SO_2 (3.10–4.49 Å),[15] confirming the very efficient packing of SO_2 molecules within this material, leading to high storage capacity and density. Indeed, at 298 K and 1 bar the density of adsorbed SO_2 in MFM-300(In) was estimated to be 1.27 g cc^{-1}, comparable to the liquid SO_2 density of 1.46 g cc^{-1} at 263 K and 1 bar. Attempts to locate the adsorbed CO_2 molecules in MFM-300(In) at 298 K suffered from serious positional disorder in the refinement, consistent with the low Q_{st} and hence reduced strength of binding. The location of adsorbed CO_2 molecules was therefore determined at 195 K where thermal motion is greatly reduced. Similarly, two independent CO_2 adsorption sites (CO_2^I and CO_2^{II}) were found in CO_2-loaded MFM-300(In) at 195 K (Figure 2d–f). CO_2^I was located near to the bridging hydroxyl group [O=C=O^I···O−H = 3.04(1) Å] in an almost end-on configuration, disordered over a mirror plane intersecting the metal hydroxy bond, with full occupancy; CO_2^{II} was located perpendicular to CO_2^I [O=C=O^{II}···C=O^I = 3.44(4) Å], lying parallel to the pore at a distance of 3.65(3) Å to the phenyl rings, again with full occupancy. The binding distances of the adsorbed CO_2 molecules are similar to those observed in solid CO_2 (3.10 Å),[16] indicating the high packing efficiency of CO_2 at 195 K. These structural modes obtained from *in situ* diffraction studies are in excellent agreement with those obtained from DFT calculations (Figure 2c,f). This study confirms that the free bridging hydroxyl group within the pore of MFM-300(In) is the preferential binding site for both SO_2 and CO_2 molecules, followed by a secondary binding site toward the edge of the pore of this material, sitting between the phenyl rings of two discrete ligand molecules, stabilized, in principle, by an intermolecular highly cooperative dipole interaction with adsorbed gas molecules at site I. Attempts to determine the binding site for N_2 at 298 K was unsuccessful owing to the extremely low uptake observed in this material.
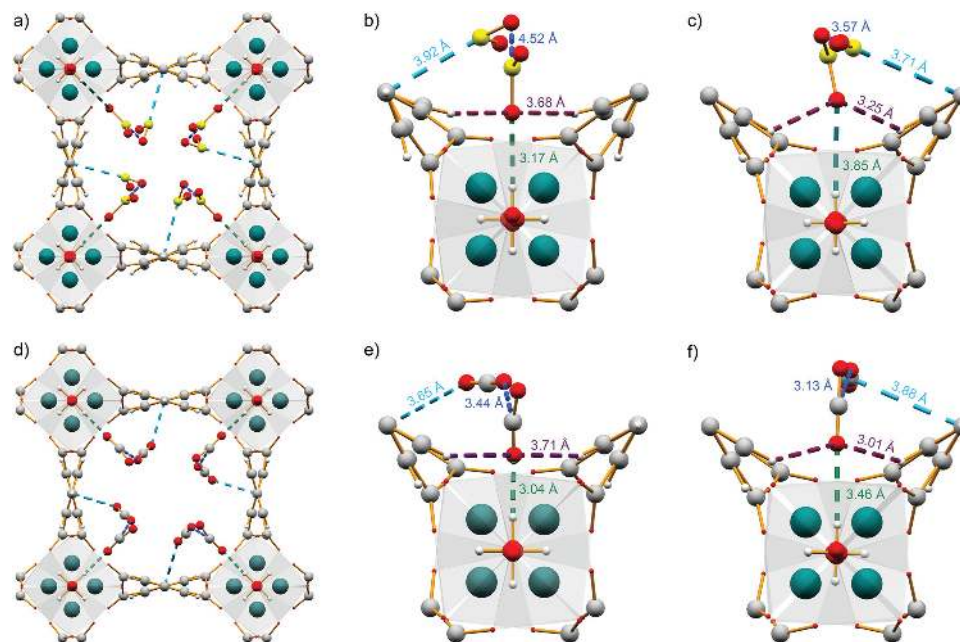
Figure 2. View of the position of adsorbed SO_2 molecules within MFM-300(In) as determined by a,b) single-crystal X-ray diffraction; c) DFT calculations. View of position of adsorbed CO_2 molecules within MFM-300(In) as determined by d,e) powder X-ray diffraction; f) DFT calculations. The $O=X=O^{I}\cdots O-H$ bond lengths are shown in green; $O=X=O^{I}\cdots H$–phenyl bond lengths are shown in purple; $O=X=O^{II}\cdots X=O^{I}$ bond lengths are shown in blue; $O=X=O^{II}\cdots$pore wall bond lengths are shown in cyan.

Understanding the change in dynamics upon the binding of gas (SO_2, CO_2, and N_2) within these materials can provide fundamental insights into the multiple supramolecular binding modes (e.g., hydrogen bond, intermolecular dipole) of the adsorbed gas molecules and therefore can give insight into the selectivity. INS is a spectroscopic technique which is particularly sensitive to the dynamics of hydrogen atoms, with signals overwhelming all other modes, and is used here to investigate the vibrational motions of the host–guest systems.[10e,12a,17] INS spectra of bare and the N_2, CO_2, and SO_2 loaded materials (2 gas molecules per In for each gas) were collected at 10 K (**Figure 3**a–c), in addition to DFT calculations of the INS spectra of these structural models, which were found to be in excellent agreement with the experimental data (Figure 3d,e). INS spectra of the bare material show three distinct low-energy peaks at 13, 22, and 31 meV (group I) relating to the lattice modes of the material; additional groups of peaks were observed at 40–70 meV (group II) and 70–167 meV (group III) and were assigned to wagging/bending modes of the bridging hydroxyl group and of the aromatic C—H bonds from the phenyl rings, respectively. On addition of N_2, peaks in groups I, II, and III remain essentially unchanged, indicating that there is negligible distortion of the local modes of the MOF material and of the O—H or C—H wagging modes, consistent with the extremely low binding energy and adsorption properties. Addition of CO_2 is accompanied by significant broadening to peaks in group I, indicating a wide range of changes to the lattice dynamic modes of the material (more stiffening) as a result of CO_2 inclusion. This is further accompanied by shifts in the peaks of group II and III, confirming that the adsorbed CO_2 molecules are strongly interacting with the bridging hydroxyl and C—H groups. The

addition of SO_2 results in even further broadening of the lattice modes, commensurate with the increased rigidity of the overall framework. The positions of peaks of group II and III shift more dramatically on addition of SO_2 than CO_2, with marked changes in the difference spectra. The changes upon addition of SO_2 indicate that the adsorbed SO_2 molecules are interacting with the bridging hydroxyl group in a much stronger fashion than that of CO_2. Interestingly, to the best of our knowledge, this represents the first example of direct observation and quantification of the host–guest binding strength via analysis of lattice dynamics in MOFs. These results confirm the changes in the host–guest dynamics upon gas binding in MFM-300(In) and thus the observed selectivities for gas separation.

In order to further investigate effects of pure component and mixed gas adsorption on the vibrational modes of this material, an in situ synchrotron micro-IR spectroscopic study[18] was carried out with single crystals of MFM-300(In) upon loading of SO_2, CO_2, and a SO_2/CO_2 mixture (Figure 3f–i). In particular, comparison of the change of $\nu(\mu_2\text{-OH})$ modes in the presence of SO_2 and CO_2 can provide a unique insight into the strength of the binding and competition between these two components within MFM-300(In). Upon desolvation of MFM-300(In) under a He flow, a broad band centered at ≈3550 cm^{-1} (corresponding to adsorbed water) was completely removed, revealing a distinct absorption band at 3657 cm^{-1} corresponding to the $\nu(\text{OH})$ stretching mode. Upon dosing the desolvated material with up to 1 bar of CO_2, this peak shifts by five wavenumbers from 3657 to 3652 cm^{-1}, indicating a partial depletion of bare —OH groups within this material, consistent with formation of the —OH$\cdots$O=C=O binding interaction, as observed in the crystallographic study. The associated combination bands of
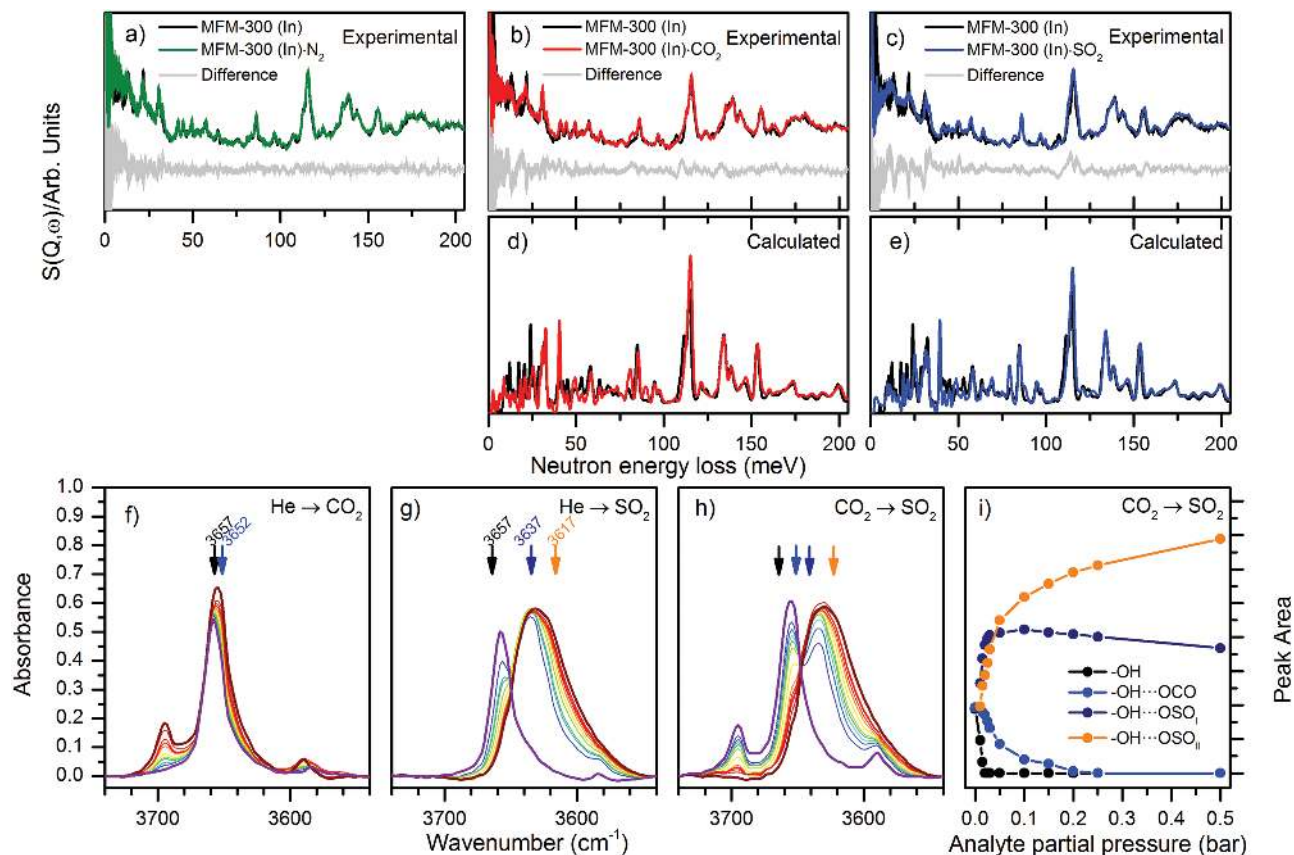
Figure 3. Views of a–c) experimental and difference INS spectra of bare, N_2, CO_2, and SO_2 loaded MFM-300(In); d,e) simulated INS spectra of bare, CO_2, and SO_2 loaded MFM-300(In); f–h) IR spectra of the $\nu(\mu_2\text{-OH})$ stretch region of MFM-300(In) for CO_2- and SO_2-loading and CO_2 displacement by SO_2; i) fitted peak areas of the $\nu(\mu_2\text{-OH})$ stretches corresponding to bare MFM-300(In) and the CO_2 and SO_2 interaction modes in the competition experiment.

adsorbed CO_2 appear at ≈3590 and 3695 cm^{-1} and appear in the same ratio as that of the −OH···O=C=O binding interaction, and in proportion to the observed CO_2 isotherm under the same conditions (Figure S25, Supporting Information). In contrast, initial loading of SO_2 to a partial pressure of only 0.01 bar results in a significant depletion of the $\nu(OH)$ band at 3657 cm^{-1}, consistent with the sharp adsorption profile of SO_2 at this pressure and indicating that this binding site is being rapidly occupied. Depletion of the band corresponding to the $\nu(OH)$ stretching mode of the bare material is accompanied by the emergence of a new band at 3637 cm^{-1}, a 20 cm^{-1} red shift from the original band, indicating a significant change to the −OH mode upon SO_2 binding. Indeed, upon additional loading of SO_2 from 0.01 to 1 bar, a second new band grows in steeply at 3617 cm^{-1} with concomitant loss of the original bare $\nu(OH)$ band and gradual decrease of the $\nu(OH\cdots O=S=O^I)$ band shifted ≈40 cm^{-1} lower energy than the original bare $\nu(OH)$ band, corresponding to the populating of the secondary binding site (II) by SO_2 molecules. We tentatively ascribe this additional shift to the second SO_2 molecule at site II affecting the $\nu(OH)$ mode through the SO_2 molecule at the first binding site I, i.e., in a In−OH···O=S=O^I···S=O^{II} manner. The shift of this second band is consistent with the electron-withdrawing nature of such an interaction on the −OH group. Upon reduction of SO_2 partial pressure (by adding a He carrier flow), the IR spectra confirmed the rapid removal of

bound SO_2 molecules in the pore and the return of the $\nu(OH)$ mode to its original position at 3657 cm^{-1}, thus confirming the efficient regeneration of MFM-300(In) post adsorption of SO_2.

The unique insight into the population of CO_2 and SO_2 molecules bound within this material makes the IR microscopic approach ideal to directly investigate the competitive binding of SO_2/CO_2 mixtures, by direct quantification of the gas mixture present at a range of concentrations. This information is difficult to achieve by crystallographic means due to the positional disorder of the guest species. In order to determine the proportion of SO_2 and CO_2 in this material in a competitive binding experiment, bare MFM-300(In) was first equilibrated with 1 bar of CO_2, followed by sequential dosing of CO_2/SO_2 mixtures containing ever higher partial pressures of SO_2. During this investigation the $\nu(OH)$ mode of this material was monitored continuously for the presence of any possible site displacement of bound CO_2 by SO_2. At 1 bar CO_2, the peak areas of the $\nu(OH)$ bands corresponding to the bare and CO_2-loaded material are approximately equal, as observed in the pure CO_2 loading experiment. Upon dosing the CO_2-loaded material with SO_2 in a stepwise manner (i.e., tuning the SO_2/CO_2 mixture composition from 0/100 to 100/0 while maintaining a total pressure of 1 bar), there is a steady change in the $\nu(OH)$ region that includes new bands appearing in a similar manner to those observed in the pure SO_2 experiment, indicating that the bound CO_2 does not

impede the adsorption of SO_2. In other words, SO_2 in the gas phase can readily displace the bound CO_2 in the pore as a result of the stronger binding strength of this gas. Fitting the $\nu(OH)$ bands determined in the pure component experiment reveals a very rapid depletion of the $\nu(OH)$ band corresponding to the bare material, reaching 0 by a SO_2 partial pressure of 0.02 bar, and a more gradual decrease of the $\nu(OH)$ band corresponding to the CO_2-occupied sites, reaching 0 at a SO_2 partial pressure of 0.25 bar. This is accompanied by concurrent increases in the SO_2-bound $\nu(OH)$ bands at both 3637 and 3617 cm^{-1}. At a SO_2 partial pressure of 0.10 bar, the band at 3637 cm^{-1} reaches its maximum intensity, indicating saturation of SO_2 at site I. The profile of the 3617 cm^{-1} band is comparable to that of the pure component SO_2 experiment, as population of SO_2 at the site II requires a SO_2 molecule residing at site I to satisfy the intermolecular dipole binding network, but the band intensity rises less steeply with increasing SO_2 partial pressure in the competition experiment, presumably as CO_2 displacement was still occurring up to 0.25 bar. This result confirms the rapid site displacement of bound CO_2 by free SO_2 in MFM-300(In) and therefore validates the exceptionally high selectivity observed for this competing mixture.

In conclusion, selective SO_2 adsorption has been realized in MFM-300(In), a material which exhibits exceptionally high SO_2/CO_2 (60), SO_2/CH_4 (425), SO_2/N_2 (5000) selectivity under ambient conditions. Importantly, MFM-300(In) displays complete retention of the framework structure upon contact with SO_2, H_2SO_3, and H_2SO_4 (Figure S1–S9, Supporting Information), demonstrating the excellent stability and applicability of this material for SO_2 capture in both dry and humid conditions. This is rare for a MOF material and especially so for an In(III) system. A combination of crystallographic and spectroscopic techniques have been applied to investigate the origin of the observed selectivity of this material, revealing that differences in the strength of multiple supramolecular binding interactions with the pore surface are directly responsible for the different binding affinity to a number of gases. Thus, high selectivity for SO_2, excellent stability and facile regeneration post-adsorption are all achieved in MFM-300(In).

Experimental Section

In Situ Synchrotron X-Ray Diffraction: High-resolution X-ray powder diffraction of SO_2 and CO_2 loaded MFM-300(In) was carried out at 0.826126(2) Å on beamline I11 of the Diamond Light Source and at 0.495891(2) Å on beamline ID31 at the European Synchrotron Radiation Facility, respectively. Single-crystal X-ray diffraction of desolvated and CO_2-loaded MFM-300 (In) was carried out at beamline I19 of the Diamond Light Source. The experiments were carried out using a custom gas cell and handling equipment. The desolvated material was generated in situ by heating the sample to 423 K under reduced pressure (10^{-6} mbar) (2 h for powdered sample, 20 h for single crystal). The samples were cooled to 298 K before being dosed with the analyte gas and in the case of CO_2, further cooled to 195 K before the diffraction data were measured. The locations of the gas molecules could be discerned from the Fourier difference maps at 298 K for SO_2 and 195 K for CO_2 and were included in the refinement model with bond distances and angles constrained to ideal values.

Crystal Data for Desolvated MFM-300(In): [(C$_{16}$H$_8$O$_6$In$_2$)]; colorless block (0.2 mm × 0.1 mm × 0.1 mm). Tetragonal, $I4_122$ (no. 98), $a = 15.4886(8)$, $c = 12.3439(13)$ Å, $V = 2961.3(4)$ Å^3, $Z = 4$, $\rho_{calcd} = 1.323$ g cm^{-3},

$\mu_{calcd} = 1.590$ mm^{-1}, $F(000) = 1128$. A total of 11489 reflections were collected, of which 1647 were unique giving $R_{int} = 0.0048$. Final R_1 (wR_2) = 0.0255 (0.0266) with GoF = 1.173. The final difference Fourier extrema were 0.63 and -0.27 eÅ^{-3}.

Crystal Data for MFM-300(In)·4CO$_2$: [(C$_{16}$H$_8$O$_6$In$_2$)·4.20CO$_2$]; colorless block ($0.2 \times 0.1 \times 0.1$ mm). Tetragonal, $I4_122$ (no. 98), $a = 15.352(12)$, $c = 12.226(13)$ Å, $V = 2882(5)$ Å^3, $Z = 4$, $\rho_{calcd} = 1.783$ g cm^{-3}, $\mu_{calcd} = 1.554$ mm^{-1}, $F(000) = 1495$. A total of 7264 reflections were collected, of which 1041 were unique giving $R_{int} = 0.032$. Final R_1 (wR_2) = 0.0277 (0.0283) with GoF = 1.223. The final difference Fourier extrema were 0.64 and -0.43 eÅ^{-3}.

Crystal Data for MFM-300(In)·4SO$_2$: [(C$_{16}$H$_8$O$_6$In$_2$)·4SO$_2$]; White powder. Tetragonal, space group $I4_122$ (no. 98), $a = 15.50965(4)$, $c = 12.31972(3)$ Å, $V = 2963.50(2)$ Å^3, $Z = 4$. The final Rietveld plot corresponds to satisfactory crystal structure model ($R_{Bragg} = 0.032$) and profile ($R_p = 0.051$ and $R_{wp} = 0.068$) indicators with a goodness-of-fit parameter of 1.57.

CCDC-1475893 to 1475895 contain the supplementary crystallographic data for this paper. These data can be obtained free of charge from the Cambridge Crystallographic Data Centre via www.ccdc.cam.ac.uk/data_request/cif.

Inelastic Neutron Scattering: INS spectra of a powdered sample of MFM-300(In) were collected in an 11 mm vanadium sample can at 10 K using the TOSCA spectrometer at the ISIS Pulsed Neutron & Muon source using the time-of-flight technique. The desolvated material was generated before loading into the instrument by heating the sample can to 403 K under reduced pressure (10^{-7} mbar) for 72 h. Gases were dosed volumetrically (N_2 at 90 K; CO_2 at 270 K and SO_2 at 290 K) from a calibrated volume. The desolvated material was regenerated between runs by heating to 373 K under reduced pressure (10^{-7} mbar) for 2 h.

Modeling of INS Spectra: Modeling of the INS spectra of bare, CO_2 and SO_2 loaded MFM-300(In) were performed using CASTEP,[19] with the generalized gradient approximation, as implemented by Perdew–Burke–Ernzerhof, used to describe the exchange-correlation interactions and norm-conserving pseudopotentials to account for the effects of core electrons. Calculations to determine the force constants and dynamical matrix were carried out using the density functional perturbation theory on an energy-minimized unit cell and used to determine the electronic structure and phonon modes. Simulated INS spectra were generated from the DFT phonon modes using aClimax.[20]

Synchrotron Microinfrared Spectroscopy: Infrared spectroscopic measurement of CO_2- and SO_2-loaded MFM-300(In) were carried out using a Bruker Hyperion3000 microscope equipped with an LN_2 cooled MCT (Mercury Cadmium Telluride) detector, coupled to a Bruker Vertex spectrometer supplied with broadband radiation from beamline B22 of the Diamond Light Source. The experiments were carried out using a Linkam FTIR600 environmental gas stage using custom gas handling equipment at a constant flow rate of 100 cm^3 min^{-1}. The desolvated sample was generated in situ by heating the sample to 393 K under a flow of dry He for 2 h, the sample was then cooled to 298 K and dosed with freshly prepared analyte gas mixtures.

SO$_2$ Safety: All systems involved in the supply, delivery and measurement of SO_2 were rigorously leak tested and used only within range of a SO_2 detection system with a sensitivity of 1 ppm. All gases exhausted from experimental apparatus were diluted with a flow of N_2 and fed into fume hood extracts.

Supporting Information

Supporting Information is available from the Wiley Online Library or from the author.

Acknowledgements

[1] World Health Organisation (WHO), *7 million premature deaths annually linked to air pollution*, http://www.who.int/mediacentre/news/releases/2014/air-pollution/en/; accessed: April 2016.

[2] Z. Chen, J. Wang, G. Ma, Y. Zhang, *Lancet* **2013**, *382*, 1959.

[3] a) J. J. Winebrake, J. J. Corbett, E. H. Green, A. Lauer, V. Eyring, *Environ. Sci. Technol.* **2009**, *43*, 4776; b) L. Schrooten, I. De Vlieger, L. I. Panis, C. Chiffi, E. Pastori, *Sci. Total Environ.* **2009**, *408*, 318; c) S. P. Schweinfurth, in *The National Coal Resource Assessment Overview (U.S. Geological Survey Professional Paper 1625-F)*, (Eds: B. S. Pierce, K. O. Dennen), U.S. Geological Survey, Reston, VA, USA **2009**, Ch. C.

[4] J.-Y. Lee, T. C. Keener, Y. J. Yang, *J. Air Waste Manage. Assoc.* **2009**, *59*, 725.

[5] a) J. H. Gary, G. E. Handwerk, *Petroleum Refining Technology and Economics, 4th Ed.*, Marcel Dekker Inc, New York **2001**; b) R. Zevenhoven, P. Kilpinen, *Control of Pollutants in Flue Gases and Fuel Gases*, Helsinki University of Technology course ENE-47.153, Ch. 3, available from: http://users.tkk.fi/Brzevenho/gasbook; accessed: April 2016.

[6] World Health Organisation (WHO), *Air Quality Guidelines for Particulate Matter, Ozone, Nitrogen Dioxide and Sulfur Dioxide*, http://apps.who.int/iris/bitstream/10665/69477/1/WHO_SDE_PHE_OEH_06.02_eng.pdf; accessed: April 2016.

[7] a) I. Matito-Martos, A. Martin-Calvo, J. J. Gutiérrez-Sevillan, M. Haranczyk, M. Doblare, J. B. Parra, C. O. Ania, S. Calero, *Phys. Chem. Chem. Phys.* **2014**, *16*, 19884; b) L. Ding, A. Ö. Yazaydin, *J. Phys. Chem. C* **2012**, *116*, 22987; c) J. Yu, Y. Ma, P. B. Balbuena, *Langmuir* **2012**, *28*, 8064; d) D. M. D'Alessandro, B. Smit, J. R. Long, *Angew. Chem., Int. Ed. Engl.* **2010**, *49*, 6058.

[8] W. Lu, Z. Wei, Z.-Y. Gu, T.-F. Liu, J. Park, J. Park, J. Tian, M. Zhang, Q. Zhang, T. Gentle III, M. Bosch, H.-C. Zhou, *Chem. Soc. Rev.* **2014**, *43*, 5561.

[9] a) K. Sumida, D. L. Rogow, J. A. Mason, T. M. McDonald, E. M. Bloch, Z. R. Herm, T.-H. Bae, J. R. Long, *Chem. Rev.* **2012**, *112*, 724; b) M. P. Suh, H. J. Park, T. K. Prasad, D.-W. Lim, *Chem. Rev.* **2012**, *112*, 782; c) E. Barea, C. Montoro, J. A. R. Navarro, *Chem. Soc. Rev.* **2014**, *43*, 5419; d) J.-R. Li, J. Sculley, H.-C. Zhou, *Chem. Rev.* **2012**, *112*, 869; e) S. Keskin, S. Kizilel, *Ind. Eng. Chem. Res.* **2011**, *50*, 1799.

[10] a) J. A. Mason, M. Veenstra, J. R. Long, *Chem. Sci.* **2014**, *5*, 32; b) Y. Peng, V. Krungleviviute, I. Eryazici, J. T. Hupp, O. K. Farha, T. Yildirim, *J. Am. Chem. Soc.* **2013**, *135*, 11887; c) Z. R. Herm, E. D. Bloch, J. R. Long, *Chem. Mater.* **2014**, *26*, 323; d) Y. He, W. Zhou, R. Krishna, B. Chen, *Chem. Commun.* **2012**, *48*, 11813; e) S. Yang, A. J. Ramirez-Cuesta, R. Newby, V. Garcia-Sakai, P. Manuel, S. K. Callear, S. I. Campbell, C. C. Tang, M. Schröder, *Nat. Chem.* **2015**, *7*, 121; f) S. Gao, C. G. Morris, Z. Lu, Y. Yan, H. G. W. Godfrey, C. Murray, C. C. Tang, K. M. Thomas, S. Yang, M. Schröder, *Chem. Mater.* **2016**, *28*, 2331.

[11] a) M. Savage, I. da Silva, M. Johnson, J. H. Carter, R. Newby, M. Suyetin, E. Besley, P. Manuel, S. Rudić, A. N. Fitch, C. Murray, W. I. F. David, S. Yang, M. Schröder, *J. Am. Chem. Soc* **2016**, *138*, 9119; b) J. Qian, F. Jiang, D. Yuan, M. Wu, S. Zhang, L. Zhang, M. Hong, *Chem. Commun.* **2012**. *48*, 9696.

[12] a) S. Yang, J. Sun, A. J. Ramirez-Cuesta, S. K. Callear, W. I. F. David, D. P. Anderson, R. Newby, A. J. Blake, J. E. Parker, C. C. Tang, M. Schröder, *Nat. Chem.* **2012**, *4*, 887; b) S. Yang, L. Liu, J. Sun, K. M. Thomas, A. J. Davies, M. W. George, A. J. Blake, A. H. Hill, A. N. Fitch, C. C. Tang, M. Schröder, *J. Am. Chem. Soc.* **2013**, *135*, 4954; c) D. Britt, D. Tranchemontagne, O. M. Yaghi, *Proc. Natl. Acad. Sci. USA* **2008**, *105*, 11623; d) P. K. Thallapally, R. K. Motkuri, C. A. Fernandez, B. P. McGrail, G. S. Behrooz, *Inorg. Chem.* **2010**, *48*, 4909.

[13] C. P. Krap, R. Newby, A. Dhakshinamoorthy, H. García, I. Cebula, T. E. Easun, M. Savage, J. E. Eyley, S. Gao, A. J. Blake, W. Lewis, P. H. Beton, M. R. Warren, D. R. Allan, M. D. Frogley, C. C. Tang, G. Cinque, S. Yang, M. Schröder, *Inorg. Chem.* **2016**, *55*, 1076.

[14] a) N. F Cessford, N. A. Seaton, T. Düren, *Ind. Eng. Chem. Res.* **2012**, *51*, 4911; b) J. M. Simmons, H. Wu, W. Zhou, T. Yildirim, *Energy Environ. Sci.* **2011**, *4*, 2177; c) S. Xiang, Y. He, Z. Zhang, H. Wu, W. Zhou, R. Krishna, B. Chen, *Nat. Commun.* **2012**, *3*, 954.

[15] B. Post, R. S. Schwartz, I. Fankuchen, *Acta Crystallogr.* **1952**, *5*, 372.

[16] A. Simon, K. Peters, *Acta Crystallogr.* **1980**, *B36*, 2750.

[17] S. Yang, A. J. Ramirez-Cuesta, M. Schröder, *Chem. Phys.* **2013**, *428*, 111.

[18] A. Greenaway, B. Gonzalez-Santiago, P. M. Donaldson, M. D. Frogley, G. Cinque, J. Sotelo, S. Moggach, E. Shiko, S. Brandani, R. F. Howe, P. A. Wright, *Angew. Chem., Int. Ed. Engl.* **2014**, *53*, 13483.

[19] S. J. Clark, M. D. Segall, C. J. Pickard, P. J. Hasnip, M. J. Probert, K. Refson, M. C. Payne, *Z. Kristallogr.* **2005**, *220*, 567.

[20] A. J. Ramirez-Cuesta, *Comput. Phys. Commun.* **2004**, *157*, 226.